World Journal of Engineering and Technology, 2022, 10, 656-677
https://www.scirp.org/journal/wjet
ISSN Online: 2331-4249
ISSN Print: 2331-4222

Dynamic Characteristics of Metro Vehicle under Thermal Deformation of Long-Span Cable-Stayed Bridge

Quanming Long*, Qianhua Pu, Wenhao Zhou, Li Zhu, Zhaowei Chen

Mechatronics and Vehicle Engineering, Chongqing Jiaotong University, Chongqing, China
Email: *lqm_cqjtu@163.com

How to cite this paper: Long, Q.M., Pu, Q.H., Zhou, W.H., Zhu, L. and Chen, Z.W. (2022) Dynamic Characteristics of Metro Vehicle under Thermal Deformation of Long-Span Cable-Stayed Bridge. *World Journal of Engineering and Technology*, **10**, 656-677.
https://doi.org/10.4236/wjet.2022.103043

Received: July 23, 2022
Accepted: August 26, 2022
Published: August 29, 2022

Abstract

In order to study the influence of thermal deformation of long-span cable-stayed bridge (LSCSB) on the dynamic characteristics of metro vehicle on the bridge, based on the theory of vehicle-track coupled dynamics, the rigid-flexible coupled dynamic model of metro vehicle-track-LSCSB system is established by using finite element method and multi-rigid-body dynamics. Adopting this model, the deformation of LSCSB subject to temperature is analyzed, then the comprehensive effect of track random irregularity and rail deformation caused by temperature load is considered to study the dynamic characteristics of metro vehicle running through the bridge, and finally the influences of temperature increment and running speed on concerned dynamic indices of vehicle are studied. The results show that the LSCSB deforms obviously subject to temperature load, and the overall performance is that the cooling is arched, and the heating is bent, and the shape variable changes almost linearly with the temperature load. According to the parameters studied in this paper, the rail deformation caused by temperature load increases the wheel-rail vertical force, derailment coefficient and wheel load reduction rate by 1.5%, 3.1% and 5% respectively. The vertical acceleration of the vehicle body decreases by 2.4% under the cooling condition, while increases by 3.7% under the heating condition. The dynamic response of the bridge changes under temperature load. The maximum vertical and horizontal displacement in the middle of the main beam span are 6.24 mm and 2.19 mm respectively, and the maximum vertical and horizontal acceleration are 1.29 cm/s^2 and 2.54 cm/s^2 respectively. The derailment coefficient and vertical acceleration of vehicle body are more affected by temperature load, and the wheel load reduction rate and wheel-rail vertical force are more affected by speed. The conclusion of this paper provides a reference for subsequent scholars to study the influence of thermal deformation on the dynamic response of vehicles on LSCSB.

Keywords

Vehicle Engineering, Vehicle Rail Bridge Coupling Vibration, LSCSB, Temperature Load, Dynamic Characteristics

1. Introduction

With the development of science and technology, rail transit has become an important mode of transportation. The development of rail transit affects the sustainable development of a city. Some cities in some areas of our country need to build long-span bridges to achieve the purpose of traffic because of geographical conditions. Cable-stayed bridge is the main type of super long-span bridge. With the increase of span, the structure becomes more complex [1]. However, the stability of LSCSB is greatly affected by external environmental factors, especially the effect of temperature load. Under the influence of temperature, the main beam will have a large vertical deformation, which will cause the deformation of track structure on the bridge, and then affect the dynamic characteristics of rail vehicles [2]. In serious cases, it may also lead to safety accidents [3]. Therefore, it is urgent to study the dynamic characteristics of railway vehicles under temperature deformation of LSCSB.

At present, some scholars have made some achievements on bridge deformation and train vibration caused by temperature load. Anna Saetta *et al.* [4] proposed a numerical method for stress-strain analysis of concrete structures under time-space varying thermal load based on the finite element method, and proved the effectiveness and reliability of the numerical method in practical structural design through the analysis of an example. Zhu *et al.* [5] studied the interface damage evolution of slab track under the joint action of temperature change and vehicle dynamic load and its impact on dynamic response. The analysis showed that the precast slab had lateral warpage, resulting in serious longitudinal interface damage on both sides of slab track during the temperature drop process. Hambly *et al.* [6] studied how to calculate the temperature induced stress in simply supported and continuous structures according to the temperature distribution. Scanlan *et al.* [7] proposed a structural analysis method based on flutter derivative formula for the aeroelastic response of cable-stayed bridges to wind. Combined with examples, it is concluded that the analysis method can be successfully used to explain the phenomena observed in full-scale tests and practices. Xu *et al.* [8] proposed a dynamic analysis framework of train cable-stayed bridge coupling system under crosswind, and then applied the framework to a practical LSCSB. The final results show that the framework and the corresponding computer program can effectively predict the dynamic response of train cable-stayed bridge coupling system under crosswind. Hu *et al.* [9] reviewed the latest design practices of some special bridges in China's high-speed railway projects, classified them according to the length of the main span, summarized the key technical characteristics of long-span high-speed railway bridges, and discussed the feasibility of long-span high-speed railway bridges. The bridge model established by previous scholars using finite element method is rarely verified by field tests, and the accuracy of its simulation needs to be discussed. This paper verifies that the model meets the simulation requirements through field tests. Previous studies have mainly studied the dynamic response of vehicles and bridges on the bridge separately. This paper comprehensively studies the dynamic response of the bridge under external excitation. For the research of vehicle dynamic response on LSCSB, predecessors have proposed a variety of different external excitation and excitation treatment methods. This paper mainly studies the influence of temperature load on the system.

On the basis of previous studies, based on the dynamic theory of vehicle track coupling system [2], this paper establishes the finite element model of LSCSB with the actual engineering background, and then explores the action law of temperature load on LSCSB based on the thermodynamic principle [10]. By establishing the rigid-flexible coupling dynamic model of vehicle track bridge, study the influence of temperature load on vehicle dynamic response, explore the influence law of temperature load and speed on vehicle operation index, and draw relevant conclusions, which can provide some reference for subsequent research.

2. Vehicle Track Bridge Coupling Dynamic Model Considering Temperature Effect

Based on the vehicle-track coupling dynamics theory, a rigid-flexible coupling model of metro vehicle-track-LSCSB is established. The model includes vehicle subsystem model, track subsystem model and Bridge subsystem model, and the wheel-rail interaction and bridge rail interaction are used to connect the subsystems [11].

2.1. Vehicle Dynamics Model

The vehicle model is composed of car body, bogie, wheelset and suspension system. The suspension system is simulated by spring and damping. The vehicle body, bogie and wheelset have five degrees of freedom: lateral movement, heave, roll, nod and shake head. A vehicle subsystem model includes one vehicle body, two frames and four wheelsets. Therefore, the vehicle subsystem dynamics model has a total of 35 degrees of freedom [2]. **Table 1** shows the degrees of freedom of the vehicle subsystem model. **Figure 1** is the dynamic model of vehicle subsystem.

The vibration differential equation of vehicle subsystem is:

$$M_v \ddot{X}_v + C_v \dot{X}_v + K_v X_v = F_{vr} \tag{1}$$

where, M_v, C_v, K_v are the total mass matrix, total damping matrix and total

Table 1. DOF of vehicle subsystem model.

DOF	Lateral movement	Heaving movement	Rolling	Yawing	Rotation
Car body	Y_{C}	Z_{C}	ϕ_{C}	β_{C}	ψ_{C}
Framework	$Y_{\mathrm{t}i}$	$Z_{\mathrm{t}i}$	$\phi_{\mathrm{t}i}$	$\beta_{\mathrm{t}i}$	$\psi_{\mathrm{t}i}$
Wheelset	$Y_{\mathrm{w}i}$	$Z_{\mathrm{w}i}$	$\phi_{\mathrm{w}i}$	$\beta_{\mathrm{w}i}$	$\psi_{\mathrm{w}i}$

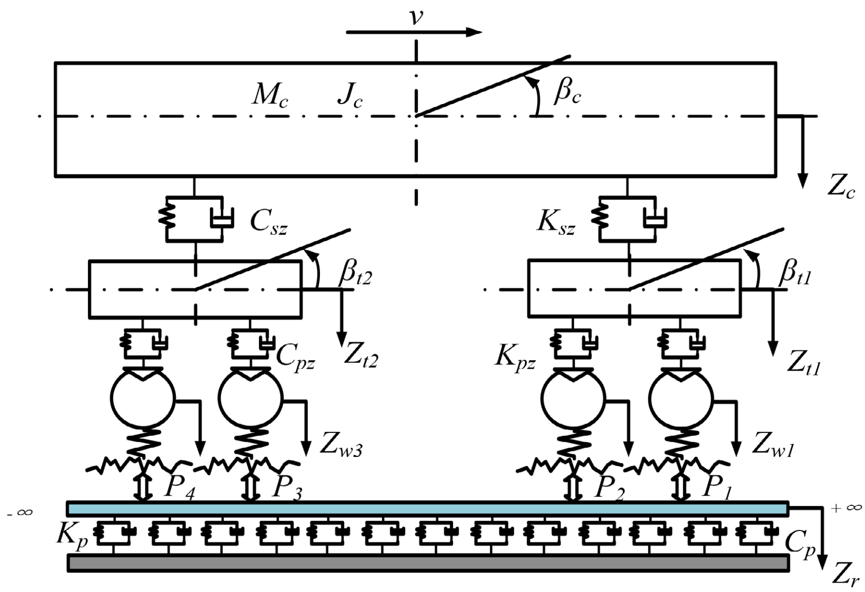

Figure 1. Dynamic model of vehicle subsystem.

stiffness matrix of the vehicle subsystem, respectively. Where, $\ddot{X}_v, \dot{X}_v, X_v, F_{vr}$ are the acceleration, speed, displacement and the force of the track subsystem on the vehicle subsystem, respectively [12].

2.2. Track Subsystem Model

The rail is simulated by Euler Bernoulli beam element [13]. The discrete elastic coefficient and viscous damping coefficient between rail and track plate are respectively K_d and C_d, from the vibration equation of Euler Bernoulli beam, the vibration differential equation of track subsystem is:

$$\begin{cases} M_r\ddot{X}_r + C_r\dot{X}_r + K_rX_r = F_{rv} + F_{rg} \\ M_g\ddot{X}_g + C_g\dot{X}_g + K_gX_g = F_{gr} + F_{gb} \end{cases} \tag{2}$$

where, M_r, C_r, K_r are the total mass matrix, total damping matrix and total stiffness matrix of the rail, respectively. Where, M_g, C_g, K_g are the total mass matrix, total damping matrix and total stiffness matrix of the track plate, respectively. Where, $\ddot{X}_r, \dot{X}_r, X_r$ are acceleration, speed and displacement of rail. Where, $\ddot{X}_g, \dot{X}_g, X_g$ are acceleration, velocity and displacement of track plate. Where, F_{rv}, F_{gb} are the force of the vehicle subsystem on the rail and the force of the bridge subsystem on the track slab; F_{rg} and F_{gr} are fastener force and its reaction force.

2.3. Bridge Subsystem Model

The bridge subsystem model is established based on the finite element theory, and its vibration differential equation is:

$$M_b\ddot{X}_b + C_b\dot{X}_b + K_bX_b = F_{bg} \tag{3}$$

where, M_b, C_b, K_b are the total mass matrix, total damping matrix and total stiffness matrix of the bridge beam subsystem, respectively. Where, $\ddot{X}_b, \dot{X}_b, X_b, F_{bg}$ are the acceleration, velocity, displacement of the bridge beam subsystem and the force of the track plate subsystem on the bridge beam subsystem [13].

The structural damping of the bridge is simulated by Rayleigh damping, and the Rayleigh damping formula is:

$$C = \alpha M + \beta K \tag{4}$$

where M and K are the mass matrix and stiffness matrix of the bridge structure respectively, and

$$\begin{cases} \alpha = 2\omega_1\omega_2 \dfrac{\xi_2\omega_1 - \xi_1\omega_2}{\omega_1^2 - \omega_2^2} \\ \beta = 2\dfrac{\xi_1\omega_1 - \xi_2\omega_2}{\omega_1^2 - \omega_2^2} \end{cases} \tag{5}$$

where, ω_1, ω_2, ξ_1 and ξ_2 are the first-order and second-order natural vibration frequencies of the structure and their corresponding damping ratios, respectively. For rigid bridges, ξ_1 and ξ_2 generally 2% ~ 3%. Therefore, as long as the stiffness matrix and mass matrix of the bridge structure are obtained, the damping matrix of the bridge structure can be obtained [12].

2.4. Rigid-Flexible Coupling Model of Vehicle Track Bridge

The vehicle, track and bridge are regarded as a coupled dynamic system, with wheel-rail contact as the interface, which is connected through the geometric compatibility conditions and interaction force balance conditions of wheel-rail [14].

Based on the above equations, the motion equation of vehicle track bridge coupling system is:

$$M\ddot{X} + C\dot{X} + KX = F \tag{6}$$

where $M = diag\left[M_v \quad M_r \quad M_g \quad M_b\right]$; $C = diag\left[C_v \quad C_r \quad C_g \quad C_b\right]$; $K = diag\left[K_v \quad K_r \quad K_g \quad K_b\right]$; $\ddot{X} = \left\{\ddot{X}_v \quad \ddot{X}_r \quad \ddot{X}_g \quad \ddot{X}_b\right\}^{\mathrm{T}}$; $\dot{X} = \left\{\dot{X}_v \quad \dot{X}_r \quad \dot{X}_g \quad \dot{X}_b\right\}^{\mathrm{T}}$; $X = \left\{X_v \quad X_r \quad X_g \quad X_b\right\}^{\mathrm{T}}$; $F = \left\{F_{vr} \quad F_{rv} + F_{rg} \quad F_{gr} + F_{gb} \quad F_{bg}\right\}^{\mathrm{T}}$.

2.5. Track Excitation Model

It is very important to correctly describe and reasonably select the track excitation model for the study of vehicle-track-bridge dynamic interaction [3]. Due to the rail deformation caused by temperature load, the actual track excitation can be expressed as:

$$Z_r = Z_{r0} + Z_{rT} \tag{7}$$

where Z_{r0} means random irregularity of the line, Z_{rT} represents the rail deformation caused by temperature load.

1) According to the comparison between the maximum running speed of vehicles allowed by different levels of lines and the actual situation, this paper uses the American level 5 track irregularity spectrum to generate the random irregularity sample of track, and is Z_{r0}.

2) The temperature load causing bridge deformation mainly considers the effects of uniform temperature difference, sunshine temperature difference and cooling temperature difference. This paper only analyzes the bridge deformation caused by sunshine temperature difference under temperature load. Liu once used exponential function to describe the temperature difference distribution of concrete structure along the direction of wall and slab [15]. In view of the fact that scholars at home and abroad have expressed the temperature distribution in the direction of pier thickness and beam height of box girder bridge in the form of index, and have been verified by a large number of experimental data. This paper intends to analyze and study the temperature distribution of box girder along the direction of beam height in the form of index [16]. Preliminarily fit the temperature distribution form in the height direction of the main beam and box girder according to the index curve, as shown in the following formula:

$$T_y = T_0 \mathrm{e}^{-ay} \tag{8}$$

where, T_y and T_0 are the temperature difference between the position of the observation point and the beam height direction respectively, y represents the distance from the observation point to the upper surface, and a is the coefficient. T_0 and a can be selected according to the code for design of reinforced concrete and prestressed concrete structures of Railway Bridges and culverts tb1002.3-2005, taking 20˚C and 5 m^{-1} respectively [17].

The temperature difference along the thickness curve of the box girder can be calculated according to the following formula:

$$T'_y = T'_0 \mathrm{e}^{-a'y} \tag{9}$$

$$T'_0 = T_0 \left(1 - \mathrm{e}^{-a\delta}\right) \tag{10}$$

where δ is the plate thickness, which a' is selected according to **Table 2**.

Based on the principle of energy conservation and heat balance equation [18], the structure can be obtained by thermodynamic analysis of the above temperature difference load by using the finite element method, can be obtained Z_{rT}.

Table 2. Index a' along the temperature difference curve of plate thickness.

Plate thickness δ/m	0.16	0.18	0.2	0.24	≥0.26
a'	15	14	13	11	10

3. Research Object and Field Modal Test

3.1. System Parameters of Metro Vehicle-Track-LSCSB

In this paper, the Dongshuimen Yangtze River Bridge of Chongqing Rail Transit Line 6 is taken as the research object. The operating model is type B vehicle, and its vehicle dynamic parameters are shown in Table 3.

Dongshuimen Yangtze River Bridge is a river crossing channel connecting Yuzhong District and Nan'an District in Chongqing, China. The upper layer of the bridge deck is a two-way four lane urban expressway, and the lower layer is a double track urban rail transit, that is a highway rail dual-purpose bridge. The total length of the bridge is 858 m. The span from the south bank to Yuzhong is (222.5 + 445 + 190.5 m). The double main tower design is adopted, in which the total height of the south tower is 172.61 m and the total height of the North Tower is 162.49 m. The bridge layout is shown in Figure 2. The sections of the

Table 3. Dynamic parameters of type b metro vehicles.

Parameter	Value	Unit
Length between truck centers	15.7	m
Wheelbase	2.5	m
Diameter of rolling circle	0.42	m
Car body mass	41.61	t
Frame mass	4.28	t
Wheelset and axle box mass	1.86	t
Car body moment of inertia	1708.23	$t{\cdot}m^2$
Frame moment of inertia	2.486	$t{\cdot}m^2$
Wheelset moment of inertia	1.036	$t{\cdot}m^2$
Primary suspension stiffness	1.07	M·n/m
Secondary suspension stiffness	0.155	M·n/m

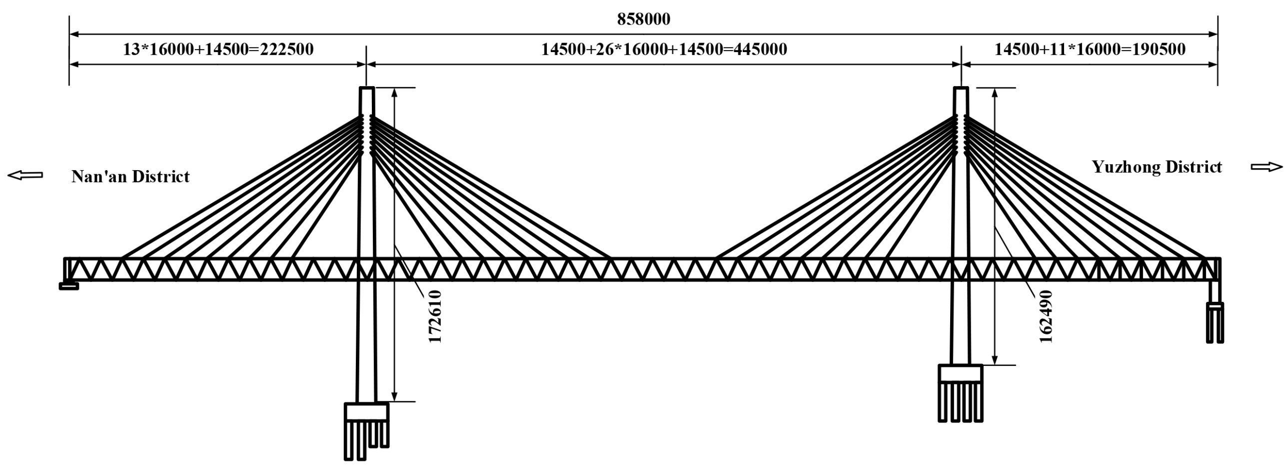

Figure 2. Layout of Dongshuimen Yangtze river bridge.

bridge are shown in Figures 3(a)-(c).

60 kg/m rail is selected for Metro Line 6, and its main parameters are shown in Table 4.

The spatial finite element model of the bridge is established based on the finite element theory [19], as shown in Figure 4. Among them, the main truss beam,

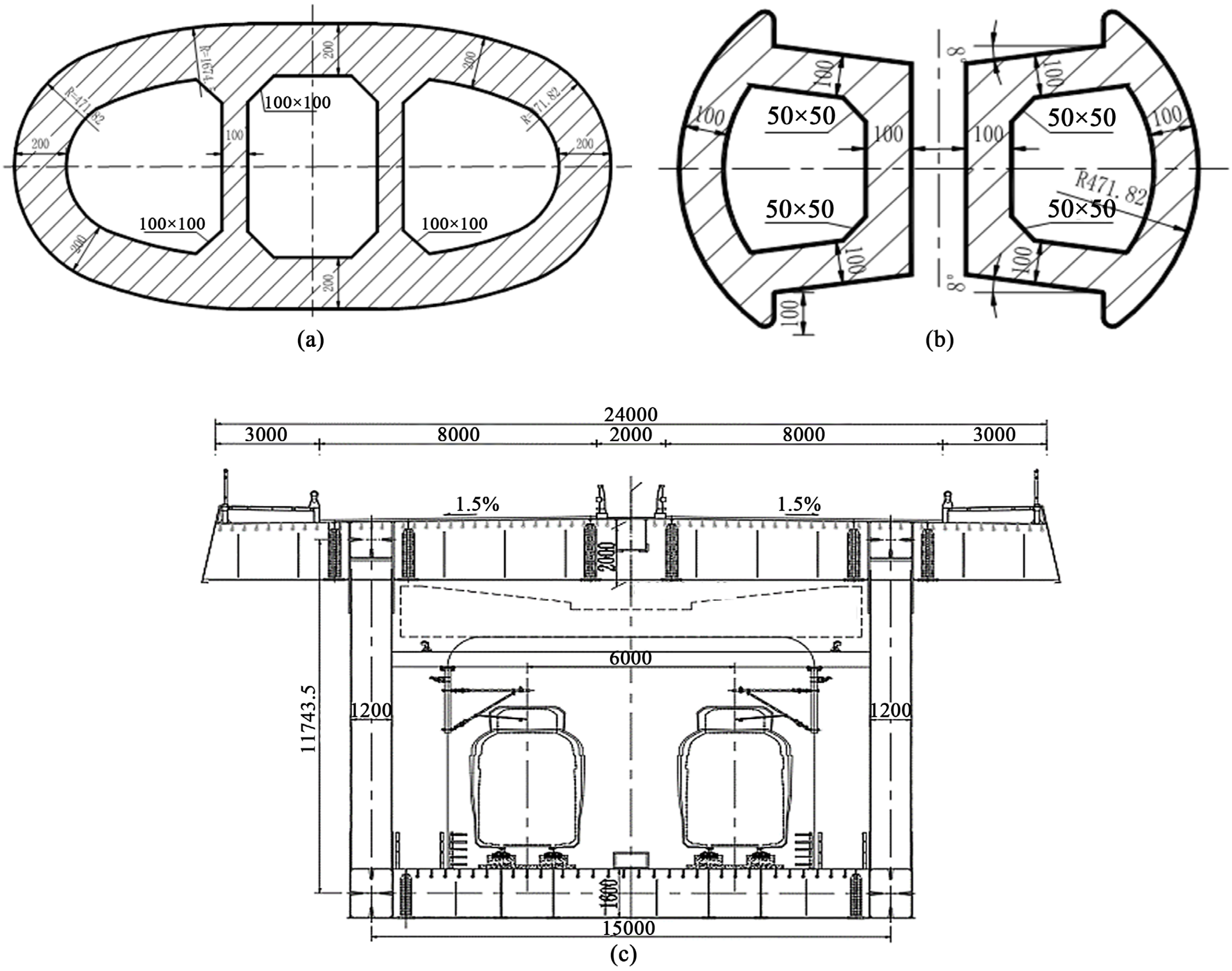

Figure 3. Bridge section. (a) Cross section of tower pier; (b) Section of tower column; (c) Section of large beam in no cable area.

Table 4. Main parameters of rail.

Parameter	Value	Unit
Elastic modulus	2.06×10^5	MPa
Poisson's ratio	0.3	/
Density	7830	kg/m^3
Top width	73	mm
Bottom width	150	mm
Height	176	mm
Waist thickness	16.5	mm

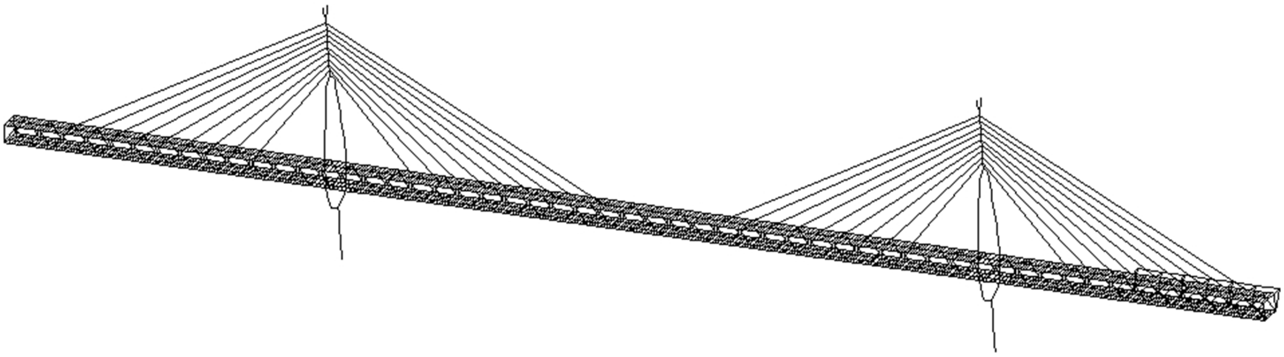

Figure 4. Finite element model of Dongshuimen Yangtze river bridge.

web member and bridge tower are simulated by beam element beam188. The main truss beam body is connected by beam element beam4 as rigid arm, and the stay cable is simulated by rod element link8. The longitudinal support system of the main bridge is arranged to set fixed hinge bearings at the fulcrum of the bridge tower. And the other piers and abutments are set with longitudinal movable hinge bearings, that is, release the longitudinal constraints.

3.2. Experimental Study on Natural Vibration Characteristics of LSCSB and Model Verification

The natural vibration characteristic of the bridge not only represents the stiffness index of the bridge, but also is an important factor in the dynamic response of the vehicle bridge coupling system [20]. The natural frequency test of Dongshuimen Yangtze River Bridge, namely the bridge modal monitoring test, can verify the accuracy of the bridge finite element model. Through the comparison and analysis between the bridge natural frequency tested on site and the corresponding vibration mode frequency of the bridge finite element simulation model. The error is within a reasonable range and the accuracy of subsequent numerical calculation is ensured [21].

The natural vibration test site of the bridge in this paper is the upper deck of Dongshuimen Yangtze River Bridge. The test section is arranged at the middle section of the secondary side span and the middle span. And the test points are arranged by three survey lines, namely, the upper, middle and lower reaches. The test instrument is a capacitive acceleration sensor. The main principle is the driving excitation method, that is to identify the structural natural vibration characteristic parameters through the residual vibration signal of the bridge structure caused by the vehicle leaving the bridge deck. The field test is shown in **Figure 5**.

The subspace iteration method is used to calculate the modal analysis of the bridge model. The first 20 frequencies are calculated, and the first 4 frequencies are compared with the measured frequencies. **Table 5** shows that the measured vibration mode of Dongshuimen Yangtze River Bridge is basically consistent with the calculated vibration mode of the finite element simulation model. Its further verifies the reliability of the model, so the model meets the calculation

(a) (b)

Figure 5. Field test of bridge natural frequency. (a) Sensor; (b) Signal acquisition.

Table 5. Measured and simulated vibration modes.

Number	Simulated mode	Measured vibration mode	Mode description
1			Girder horizontal bending mode
2	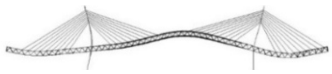		Girder vertical bending mode
3			Girder vertical bending mode
4			Girder horizontal bending mode

Table 6. Calculation frequency and measured frequency of Dongshuimen Yangtze river bridge.

Number	Calculated frequency (Hz)	Measured frequency (Hz)	Percentage (%)
1	0.313	0.350	10.5
2	0.443	0.412	7.6
3	0.580	0.651	10.9
4	0.733	0.824	11.0

requirements. **Table 6** shows the calculated and measured frequencies of Dongshuimen Yangtze River Bridge. The maximum error between the calculated frequency and the measured frequency of the bridge is 11%, and the model meets the requirements.

4. Deformation of LSCSB under Temperature Load

By consulting the relevant meteorological data to determine the temperature load, and then applying the temperature load to the bridge based on the principle of energy conservation and heat balance equation, the deformation results of the bridge can be obtained.

According to the meteorological data of Chongqing in recent ten years from 2011 to 2020, the extreme high and low temperatures of each year are sorted out as shown in **Figure 6**. The extreme low temperature in 2016 is −1˚C, and the extreme high temperature in 2011 is 42˚C.

In order to study the influence of temperature on track deformation, the overall temperature load is applied to the bridge model [22]. The extreme high and low temperatures are determined according to the meteorological data of the bridge site in recent ten years. And two temperature load cases are considered, namely, the overall temperature rise to 42˚C and the overall temperature drop to −1˚C. The simulation results show that the maximum vertical deformation at the middle of the bridge span is 227 mm under the condition of overall temperature rise. The maximum vertical deformation at the middle of the bridge span is 226 mm under the condition of overall temperature drop. The deformation amplitude of the whole bridge is almost the same under the condition of temperature rise and fall, and the direction is opposite. The whole bridge is in the state of temperature rise, deflection and arch up, as shown in **Figure 7**. The deformation law of LSCSB under temperature load is basically consistent with literature.

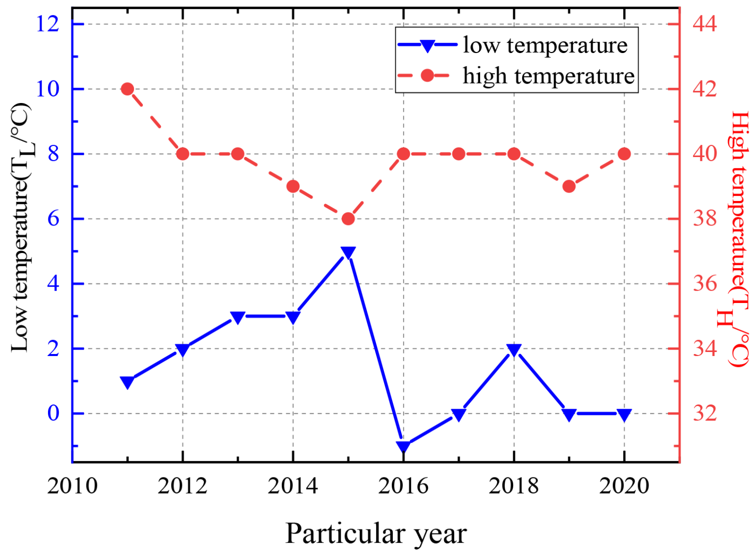

Figure 6. Distribution of extreme high and low temperatures in various years.

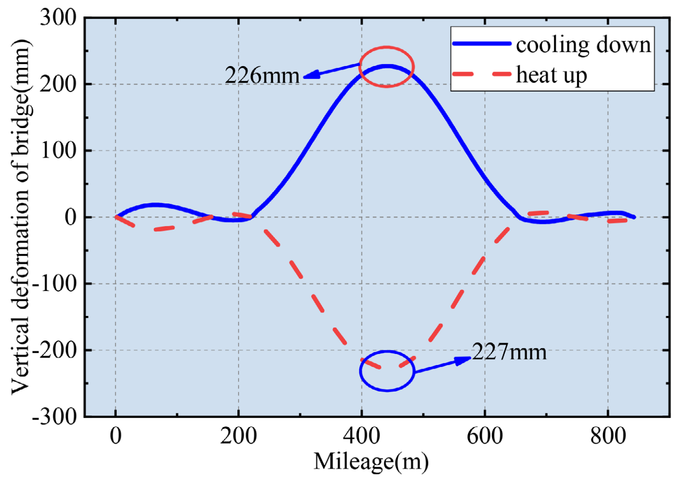

Figure 7. Vertical deformation of bridge under temperature load.

5. Dynamic Behaviors of Metro Vehicle Running through LSCSB Subject to Temperature Load

Based on the rigid-flexible coupling model of metro vehicle-track-LSCSB [16], this section explores the influence of temperature load on vehicle dynamic response and the influence law of vehicle speed and temperature load on vehicle dynamic response.

5.1. Dynamic Response of Bridge under Temperature Load

For the bridge structure, considering that the dynamic response in the middle of the main beam span is larger than that in the side span and other parts. This paper mainly gives the typical dynamic response parameters in the middle of the main beam span, that is the vertical and longitudinal acceleration and displacement in the middle of the main beam span. It can be seen from the **Figure 8** that the maximum dynamic response in the middle of the bridge span occurs when the vehicle speed is 90 km/h. The maximum vertical acceleration in the middle

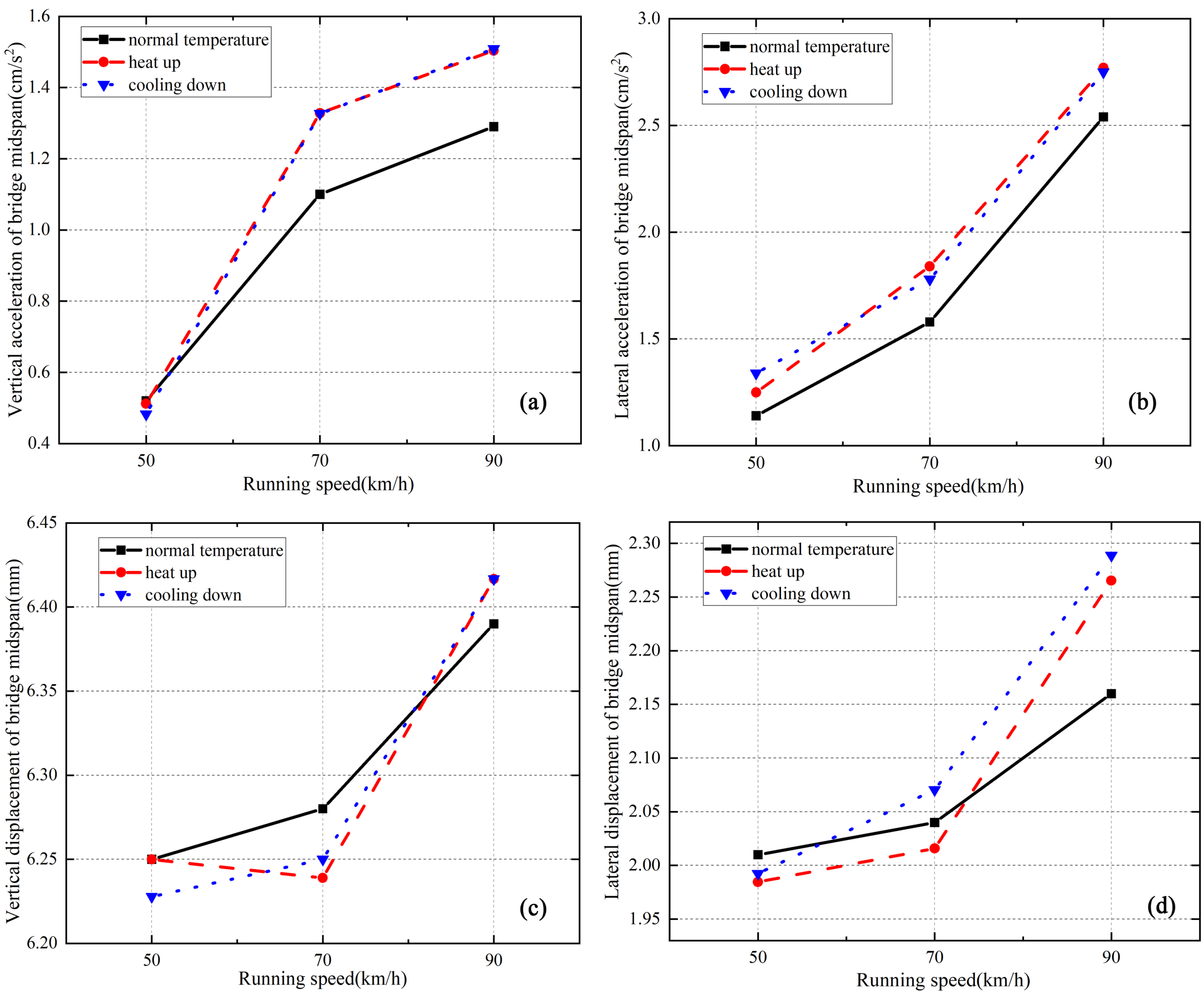

Figure 8. Dynamic response of bridge midspan under temperature load.

of the main beam span without temperature load is 1.29 cm/s^2. The maximum vertical displacement of the middle span of the main beam under the heating condition is 6.24 mm. Under the condition of no temperature load, the maximum value of transverse acceleration in the span of the main beam is 2.54 cm/s^2. The maximum lateral displacement of the middle span of the main beam under the temperature rise condition is 2.19 mm. Under the temperature and speed conditions set in this paper, the dynamic response indicators of the bridge girder midspan are more significantly affected by the speed. And the temperature rise and fall conditions have less impact on the dynamic response of the bridge.

5.2. Dynamic Response of Vehicle under Temperature Load

Since the effect of temperature load is mainly reflected in the vertical deformation of steel rail caused by the vertical deformation of the bridge, studying the influence of temperature load on the dynamic response of the train. The wheel/rail vertical force, wheel load reduction rate, derailment coefficient and vertical acceleration index when the vehicle crosses the bridge are mainly extracted, and the speed is 70 km/h. See Table 7 for the maximum value of vehicle dynamic response under temperature load.

The vertical force of wheel/rail under temperature load is shown in Figure 9. Under the initial irregularity condition, the maximum vertical wheel-rail force of

Table 7. Maximum value of vehicle dynamic response under temperature load.

Response maximum	Cooling	Normal temperature	Heat up	Limit value
Wheel/rail vertical force(kN)	95.72	94.75	95.98	170
Derailment coefficient	0.1257	0.122	0.1258	0.8
Wheel load reduction rate	0.268	0.2547	0.2672	0.6
Vertical acceleration(m/s^2)	0.3676	0.3768	0.391	1.3

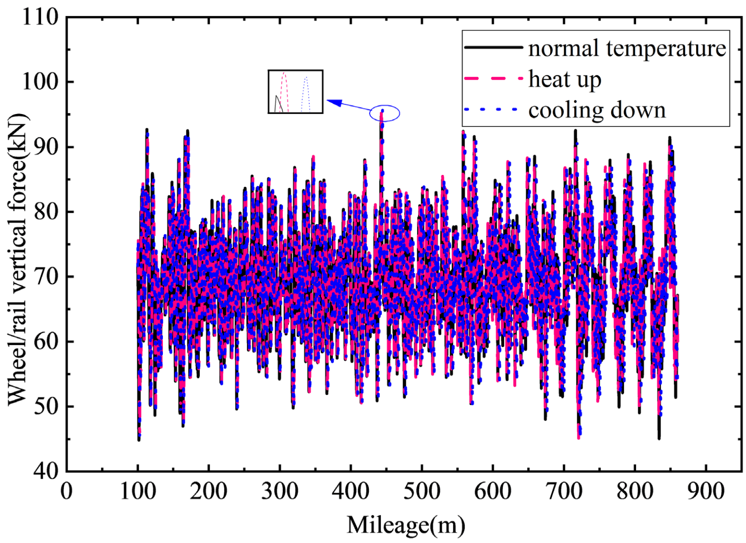

Figure 9. Wheel/rail vertical force under temperature load.

the vehicle is 94.75, 95.98 under temperature rise and 95.72 under temperature drop Compared with the derailment coefficient without temperature load. The derailment coefficient under overall temperature rise and temperature drop increases by 1.3% and 1% respectively, with a small increase and a small difference between the increase of temperature rise and temperature drop. The reason is that the track deformation caused by the overall temperature rise and fall is a smooth transition state, which has little influence on the wheel-rail vertical force.

The derailment coefficient index of vehicle is shown in **Figure 10**. Under the initial irregularity condition, the derailment coefficient of vehicle is 0.122. It is 0.1258 under temperature rise and 0.1257 under temperature drop. Due to track deformation caused by temperature rise and fall, the positions of bridges with extreme values of derailment coefficient are inconsistent. Compared with the derailment coefficient without temperature load, the derailment coefficient under overall temperature rise and temperature drop increases by 3.1% and 3% respectively, with a small difference in growth. The reason is that the track deformation amplitude caused by the overall temperature rise and fall is basically the same. Based on the above results, it can be seen that the temperature load added in this paper has little impact on the derailment coefficient index during train operation, and all of them do not exceed the safety limit of 0.8, with a large safety margin.

Calculate the wheel load reduction rate under temperature load, as shown in **Figure 11**. Under the initial rough conditions, the wheel load reduction rate of the vehicle is 0.2547, 0.2672 under the overall temperature rise and 0.268 under the overall temperature drop. Compared with the wheel load reduction rate

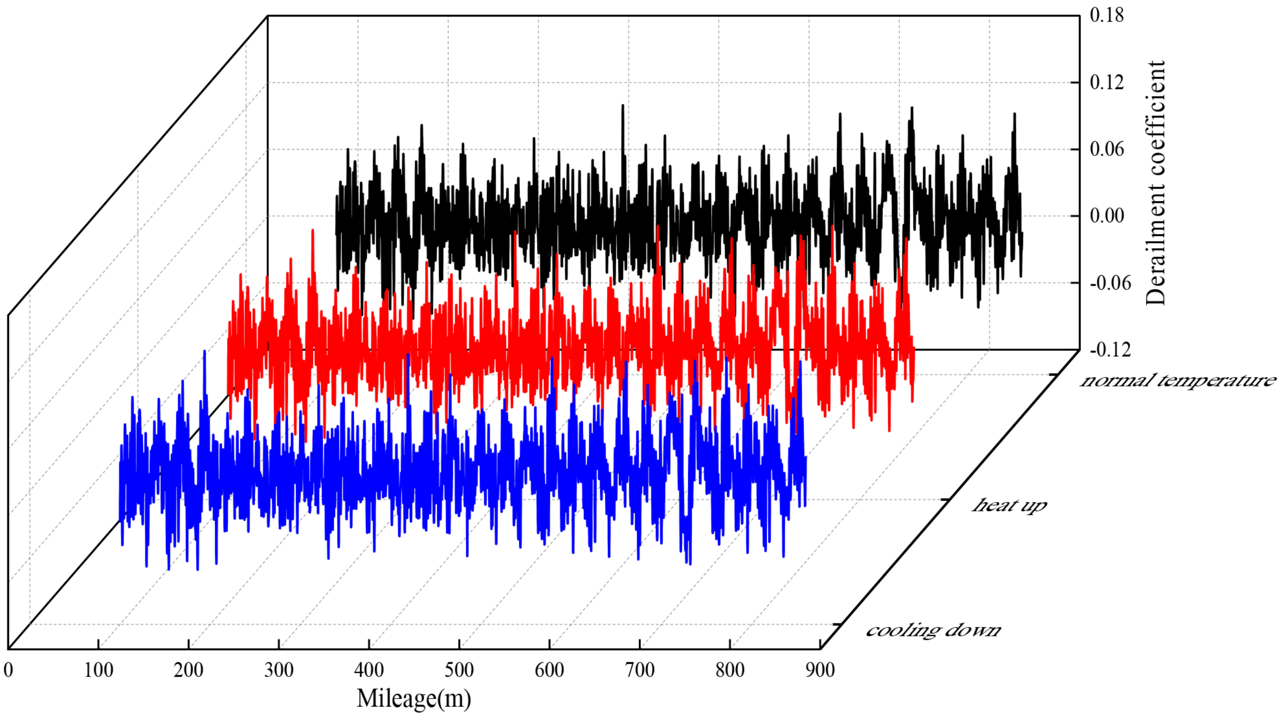

Figure 10. Derailment coefficient.

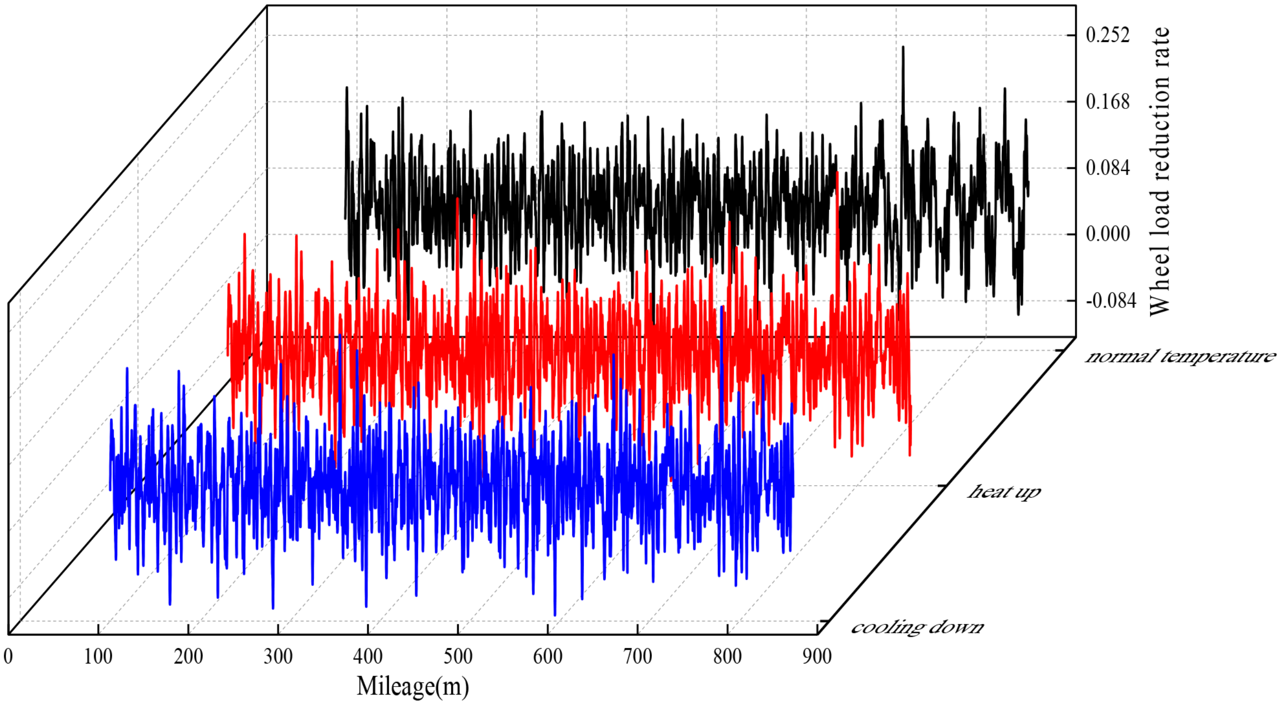

Figure 11. Wheel load reduction rate.

without temperature load, the overall temperature drop increases by 5%, and the wheel load reduction rate increases by 4.9% under the overall temperature rise. The influence of temperature load on wheel load reduction rate is greater than that of derailment coefficient. However, there is little difference in wheel load reduction rate under the condition of overall temperature rise and temperature drop. In general, under the temperature load added in this paper, the wheel load reduction rate under all working conditions is within the safety limit of 0.6, which is generally safe.

The vertical acceleration of vehicle body under temperature load is shown in Figure 12. According to the initial irregularity calculation results, the maximum vertical acceleration of the vehicle body appears at the inflection point of the bridge deformation. Which is relatively more uneven, and the maximum value is −0.3768. Under the condition of overall cooling, the vertical acceleration of the vehicle body decreases, and the maximum value is −0.3676, which decreases 2.4%. The vertical acceleration of the vehicle body increases under the overall temperature rise, with the maximum value of −0.391, an increase of 3.7%. The vertical acceleration of the vehicle body under all working conditions is far less than the safety limit of 1.3 m/s^2.

5.3. Comparison of Vehicle Dynamic Response under Different Vehicle Speed and Temperature Load

In order to study the influence of track deformation caused by temperature load on train dynamic response under different vehicle speeds. According to GB/t5599-2019, the test shall be divided into several speed levels under the maximum test speed. The increment of speed level is recommended to be 10 km/h or 20 km/h, and the allowable deviation of speed control is ±5 km/h. In this paper, 20 km/h under the maximum test speed of 90 km/h is selected as a speed level, namely 70 km/h and 50 km/h. In order to study the dynamic response of vehicles under different temperature loads and initial irregularities, six different temperature loads can be obtained by applying temperature loads of 30˚C, 20˚C and 10˚C to the whole bridge. The deformation of the bridge under temperature gradient is shown in **Figure 13**. It can be seen from the figure that the bridge shape variable is almost linearly correlated with the temperature load.

Six different temperature loads plus no temperature load, a total of 7 loading modes and 3 different running speeds are combined into 21 different working conditions. The corresponding extreme values of vehicle running dynamic response are obtained.

As can be seen from **Figure 14**, the wheel/rail vertical force of the vehicle

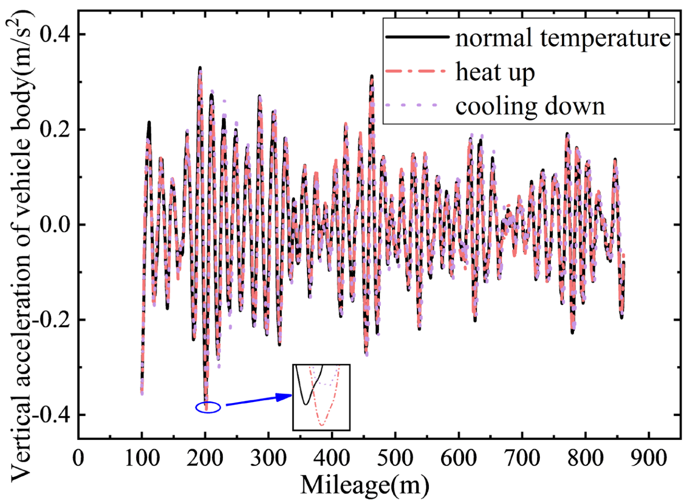

Figure 12. Vertical acceleration of vehicle body.

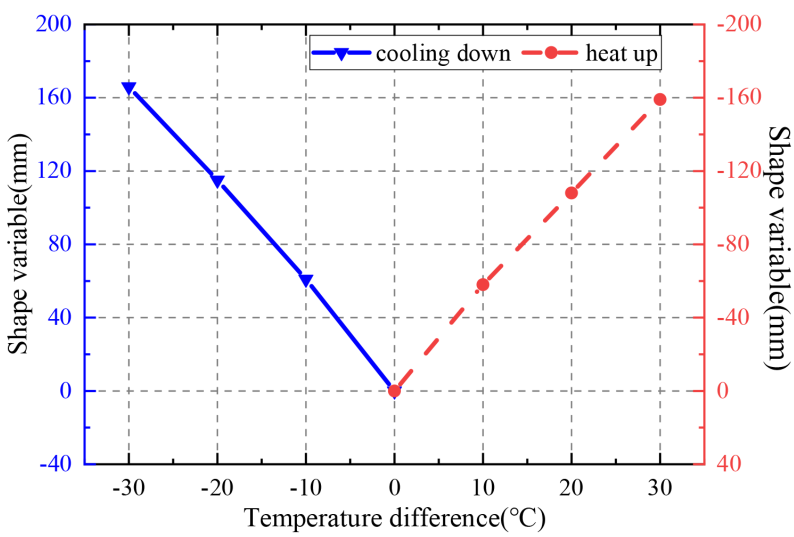

Figure 13. Bridge shape variation under temperature gradient.

increases with the increase of vehicle speed under no temperature load. It gradually increased from 92.57 kN at 50 km/h to 97.59 kN at 90 km/h, with an increase of 5.4%. At the same speed, the maximum increase rate of wheel/rail vertical force caused by temperature load is 1%, which is obtained when the speed is 70 km/h. It can be seen that the vehicle speed has a greater impact on the wheel/rail vertical force than the temperature load. When the vehicle runs at the speed of 90 km/h and the overall temperature rise of the bridge is 30˚C, the wheel-rail vertical force is 98.42 kN, which is 6.3% higher than 92.57 kN when the vehicle runs at the speed of 50 km/h and the bridge has no temperature load.

As can be seen from Figure 15, the derailment coefficient of vehicle increases with the increase of vehicle speed under no temperature load. It gradually increased from 0.1215 of 50km/h to 0.1231 of 90km/h, an increase of 1.3%, with a

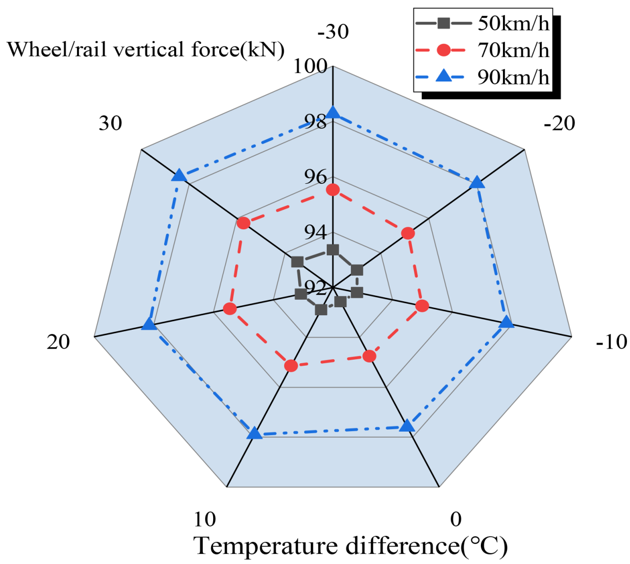

Figure 14. Wheel/rail vertical force.

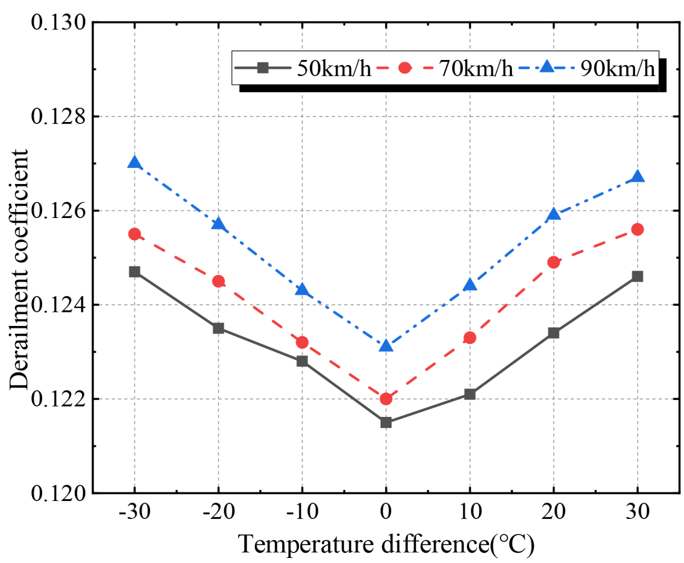

Figure 15. Derailment coefficient.

small increase. Different temperature loads lead to different track shape variables and change the derailment coefficient. With the increase of track deformation amplitude caused by temperature load, the derailment coefficient also increases, which changes almost linearly. However, there is little difference in the amplitude of track deformation caused by the same temperature, so there is little difference in the amplitude change of derailment coefficient. At the same speed, the maximum increase rate of derailment coefficient caused by temperature load is 3.1%, which is obtained when the speed is 90 km/h. It can be seen from this that temperature load has a greater influence on the derailment coefficient than vehicle speed. The maximum derailment coefficient is 0.127 when the vehicle runs at the speed of 90 km/h and the bridge is cooled by 30˚C, which is 4.5% higher than the derailment coefficient of 0.1215 when the vehicle runs at the speed of 50 km/h and the bridge has no temperature load. The derailment coefficient under each working condition is within the safety limit of 0.8, and the safety margin is large.

Figure 16 shows the comparison diagram of vehicle wheel load reduction rate under various working conditions. It can be seen from the figure that the wheel load reduction rate of the vehicle increases with the increase of vehicle speed under the initial rough conditions, from 0.2498 of 50 km/h to 0.2653 of 90 km/h, an increase of 6.2%. The track deformation caused by temperature load is a smooth curve, which has little effect on the wheel load reduction rate. At the same vehicle speed, the maximum increase rate of wheel load reduction rate caused by temperature load is 3.6%, which is obtained when the vehicle speed is 90 km/h. Therefore, the wheel load reduction rate is more affected by the speed. When the vehicle runs at the speed of 90 km/h and the overall temperature of the bridge drops by 30˚C, it can be obtained. The wheel load reduction rate is

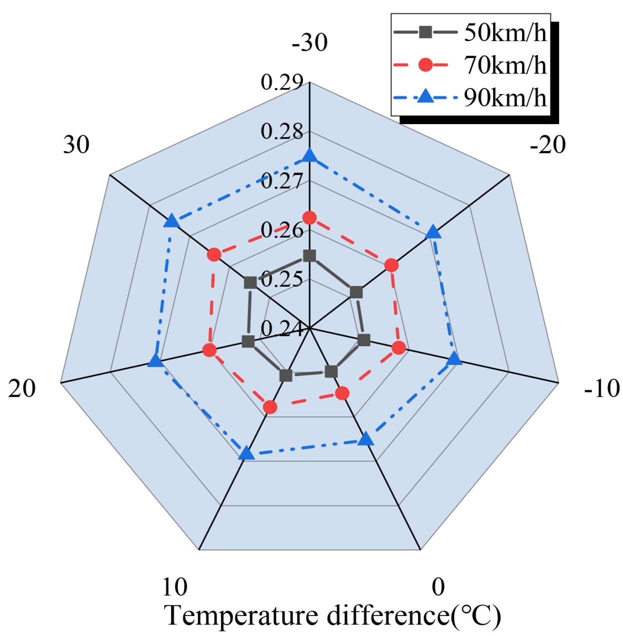

Figure 16. Wheel load reduction rate.

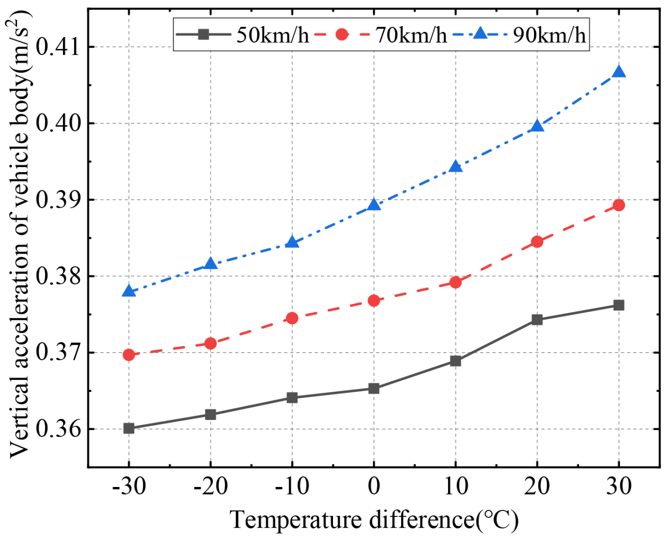

Figure 17. Vertical acceleration of vehicle body.

0.2748, which is 10% higher than the wheel load reduction rate of 0.2498 when the vehicle runs at 50 km/h and the bridge has no temperature load. However, the maximum wheel load reduction rate under all working conditions still meets the safety limit of 0.6, which can meet the safety needs.

The bridge deforms under the action of temperature load, and the beam body cambers up and deflects down. The resulting rail deformation has an impact on the vertical acceleration of the vehicle body. It can be seen from Figure 17 that the vertical acceleration of vehicle body increases with the increase of loading temperature load. Because the deformation of the bridge under temperature load is almost linear, the vertical acceleration of the vehicle body changes almost linearly at the same speed. When the vehicle speed is 50 km/h, the vertical acceleration of vehicle body under heating load and cooling load increases, the amplitude is 4.4%. When the vehicle speed is 70 km/h, the vertical acceleration of the vehicle body under heating load and cooling load increases by 5.3%. When the vehicle speed is 90 km/h, the vertical acceleration of the vehicle body under heating load and cooling load increases by 7.6%. Summarizing the above laws, it can be concluded that the greater the speed, the greater the influence of rail deformation caused by temperature load on the vertical acceleration of the vehicle body. On the whole, the increase of vehicle speed will also increase the vertical acceleration of the vehicle body.

6. Conclusions

Based on the vehicle-track coupling dynamics theory, this paper takes Dongshuimen Yangtze River Bridge as the research object, and establishes the rigid-flexible coupling dynamics model of vehicle track bridge through joint simulation. According to the principle of thermodynamics, the deformation law of LSCSB under temperature load is studied, the influence of track deformation caused by temperature load on vehicle dynamic response is analyzed. The influence law of temperature load and vehicle speed on vehicle dynamic response index is explored. The following conclusions are obtained:

1) The deformation of LSCSB under temperature load is significant. When extreme high temperature load is applied in this paper, the maximum deformation in the middle of the bridge span reaches 227 mm, and the shape variable is almost linearly related to the temperature load.

2) The dynamic response of the bridge changes under temperature load. The maximum vertical and horizontal displacement in the middle of the main beam span are 6.24 mm and 2.19 mm respectively. And the maximum vertical and horizontal acceleration are 1.29 cm/s^2 and 2.54 cm/s^2 respectively. The dynamic response index of the girder midspan is more significantly affected by the running speed of vehicles on the bridge.

3) The track deformation caused by temperature load has an impact on the dynamic response of vehicles. The main performance is that the wheel-rail vertical force increases under the load of rising and falling temperature, with an increase of 1.5% and 1% respectively. The derailment coefficient also increased, with an increase of 3.1% and 3% respectively. The wheel load reduction rate also increased, with an increase of 4.9% and 5% respectively. The vertical acceleration of the vehicle body decreases by 2.4% under the cooling load and increases by 3.7% under the heating load.

4) The influence of vehicle speed and temperature load on vehicle dynamic response has a certain law. Temperature load has a greater influence on the derailment coefficient than vehicle speed. Vehicle speed has a greater influence on wheel-rail vertical force and wheel load reduction rate than temperature load. At the same speed, the influence of temperature load on the vertical acceleration of vehicle body is almost linear.

Conflicts of Interest

The authors declare no conflicts of interest regarding the publication of this paper.

References

[1] Qin, S. and Gao, Z. (2017) Developments and Prospects of Long-Span High-Speed Railway Bridge Technologies in China. *Engineering*, **3**, 787-794. https://doi.org/10.1016/j.eng.2017.11.001

[2] Zhai, W.M. and Xia, H. (2011) Theory and Engineering Application of Train-Track-Bridge Dynamic Interaction. Science Press, Beijing.

[3] Zhai, W.M. (2020) Vehicle-Track Coupled Dynamics. Science Press, Beijing.

[4] Saetta, A., Scotta, R. and Vitaliani, R. (1995) Stress Analysis of Concrete Structures Subjected to Variable Thermal Loads. *Journal of Structural Engineering*, **121**, 446-457. https://doi.org/10.1061/(ASCE)0733-9445(1995)121:3(446)

[5] Zhu, S. and Cai, C. (2014) Interface Damage and Its Effect on Vibrations of Slab Track under Temperature and Vehicle Dynamic Loads. *International Journal of Non-Linear Mechanics*, **58**, 222-232. https://doi.org/10.1016/j.ijnonlinmec.2013.10.004

[6] Hambly, E.C. (1986) Temperature Distributions and Stresses in Concrete Bridges. *Structural Engineer*, **56A**, 588-598.

[7] Scanlan, R.H. and Jones, N.P. (1990) Aeroelastic Analysis of Cable-Stayed Bridges. *Journal of Structural Engineering*, **116**, 279-297. https://doi.org/10.1061/(ASCE)0733-9445(1990)116:2(279)

[8] Xu, Y.L., Zhang, N. and Xia, H. (2004) Vibration of Coupled Train and Cable-Stayed Bridge Systems in Cross Winds. *Engineering Structures*, **26**, 1389-1406. https://doi.org/10.1016/j.engstruct.2004.05.005

[9] Hu, N., Dai, G.L., Yan, B. and Liu, K. (2014) Recent Development of Design and Construction of Medium and Long Span High-Speed Railway Bridges in China. *Engineering Structures*, **74**, 233-241. https://doi.org/10.1016/j.engstruct.2014.05.052

[10] Yi, L.X. (2009) Design and Study of Long Span Steel Truss Arch Bridge of Dashengguan Changjiang River Bridge in Nanjing. *Bridge Construction*, 5 p.

[11] Chen, Z.W., Zhai, W.M., Cai, C.B. and Sun, Y. (2015) Safety Threshold of High-Speed Railway Pier Settlement Based on Train-Track-Bridge Dynamic Interaction. *Science China Technological Sciences*, **58**, 202-210. https://doi.org/10.1007/s11431-014-5692-0

[12] Zhai, W., Liu, P., Lin, J. and Wang, K. (2015) Experimental Investigation on Vibration Behaviour of a CRH Train at Speed of 350 km/h. *International Journal of Rail Transportation*, **3**, 1-16. https://doi.org/10.1080/23248378.2014.992819

[13] Liang, L., Li, X., Yin, J., Wang, D., Gao, W. and Guo, Z. (2019) Vibration Characteristics of Damping Pad Floating Slab on the Long-Span Steel Truss Cable-Stayed Bridge in Urban Rail Transit. *Engineering Structures*, **191**, 92-103. https://doi.org/10.1016/j.engstruct.2019.04.032

[14] Zhai, W., Han, Z., Chen, Z., Liang, L. and Zhu, S. (2019) Train-Track-Bridge Dynamic Interaction: A State-of-the-Art Review. *Vehicle System Dynamics*, **57**, 984-1027. https://doi.org/10.1080/00423114.2019.1605085

[15] Qian, Z. and Liu, Y. (2014) Temperature Field and Thermal Deformation of Steel Bridge Deck during Gussasphalt Pavement Paving. *Journal of Southeast University* (*Natural Science Edition*), **44**, 1024-1029.

[16] Zhang, N. and Xia, H. (2008) Vehicle-Bridge Interaction Analysis under High-Speed Trains. *Journal of Sound and Vibration*, **309**, 407-425. https://doi.org/10.1016/j.jsv.2007.07.064

[17] Zhu, Y., Ni, Y.Q., Jesus, A., Liu, J. and Laory, I. (2018) Thermal Strain Extraction Methodologies for Bridge Structural Condition Assessment. *Smart Materials and Structures*, **27**, Article ID: 105051. https://doi.org/10.1088/1361-665X/aad5fb

[18] Zhang, L., Ma, B., Wu, J., Li, H. and Li, G. (2018) Finite Element Analysis of Main Girder in Bridge Crane Considering Thermal-Mechanical Coupling Deformation. *Proceedings of the* 2018 3*rd Joint International Information Technology*, *Mechanical and Electronic Engineering Conference*, Chongqing, 15-16 December 2018, 15-16. https://doi.org/10.2991/jimec-18.2018.46

[19] Riedel, F.B. and Riedel, B. (2000) Monitoring the Thermal Deformation of Steel Beams via Vision Metrology. *ISPRS Journal of Photogrammetry and Remote Sensing*, **55**, 268-276. https://doi.org/10.1016/S0924-2716(00)00024-1

[20] Zhai, W.M. (1996) Two Simple Fast Integration Methods for Large-Scale Dynamic Problems in Engineering. *International Journal for Numerical Methods in Engineering*, **39**, 4199-4214. https://doi.org/10.1002/(SICI)1097-0207(19961230)39:24<4199::AID-NME39>3.0.CO;2-Y

[21] Guan, M.X. (1986) A Study on Sunshine Temperature Load of Masonry Bridges, Temperature Stress and Fissure. *China Railway Science*, 27-34.

[22] Xiang, B., Zhou, Y. and Chen, X.W. (2005) Research on the Dynamic Characteristics Monitoring System of Dongshuimen Yangtze River Bridge. *Western Transportation Science and Technology*, **11**, 46-50. (In Chinese)